

Coreset Selection for Object Detection

Hojun Lee¹ Suyoung Kim¹ Junhoo Lee¹ Jaeyoung Yoo² Nojun Kwak^{1*}
¹Seoul National University ²NAVER WEBTOON AI
{hojun815,ksyo96,mrjunoo,nojunk}@snu.ac.kr, yoojy31@webtoonscorp.com

Abstract

Coreset selection is a method for selecting a small, representative subset of an entire dataset. It has been primarily researched in image classification, assuming there is only one object per image. However, coreset selection for object detection is more challenging as an image can contain multiple objects. As a result, much research has yet to be done on this topic. Therefore, we introduce a new approach, **Coreset Selection for Object Detection (CSOD)**. CSOD generates imagewise and classwise representative feature vectors for multiple objects of the same class within each image. Subsequently, we adopt submodular optimization for considering both representativeness and diversity and utilize the representative vectors in the submodular optimization process to select a subset. When we evaluated CSOD on the Pascal VOC dataset, CSOD outperformed random selection by +6.4%p in AP_{50} when selecting 200 images.

1. Introduction

In today’s data-driven era, managing the sheer volume and variety of data presents a crucial challenge, particularly in areas like computer vision and deep learning, which deal with a tremendous amount of data [4, 22, 36]. With the advent of technologies such as autonomous vehicles and smart surveillance systems, accurate and efficient recognition of such image data has become paramount. One key strategy in managing these massive datasets involves ‘coreset selection,’ a method aimed at identifying a smaller, representative subset of the original dataset. This subset is then used to streamline complex computations and enhance processing efficiency.

However, as illustrated in Figure 1, traditional coreset selection methods are unrealistic because they were developed under the naïve assumption of a single object per image, a condition that real-world images do not often meet [1, 5, 10]. Real-world images typically contain the

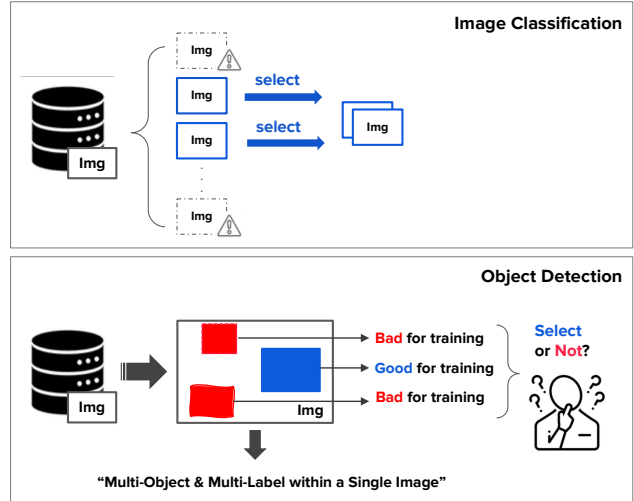


Figure 1. The difference in coreset selection between image classification and object detection.

natural variability, such as multiple objects of various categories, sizes, and locations.

This implies that we should develop methods that consider the natural variability. As Figure 1 illustrates, if we evaluate the suitability of an image on an object-by-object basis, considering one object as suitable for training does not necessarily imply that the others are also suitable. In other words, the decision of a core image should be based on all objects in an image. However, traditional methods, designed to solve only the single-image-single-object pairing, fail to consider this, and therefore struggle in realistic conditions.

In this paper, we address a significant limitation in the field of coreset selection which has traditionally operated under the assumption of a single object per image. We introduce a realistic approach tailored to the more complex, yet common, scenario where images inherently contain multiple objects. This shift from single-object to multi-object consideration is a central advancement of our work. CSOD not only recognizes the presence of numerous objects within each image but also tackles the compounded

*Corresponding author

uncertainties by considering objects’ spatial information such as size and location. To validate our method, we implemented and conducted experiments in object detection, a representative task of situations where multiple objects may reside within a single image.

Our method, CSOD, is built upon a unique concept: the ‘imagewise-classwise vector.’ To select the most representative images among compounded uncertainties, we need a way to summarize the information of each image effectively. The imagewise-classwise vector serves this purpose by averaging the features of objects of the same class within an image. This comprehensive representation allows for informed decision-making when addressing the complexities of multi-object images.

We employ a greedy approach to select individual data points sequentially by class order, thereby constructing the coreset step by step. Although this method considers only one class at each selection step, it guarantees that the most pertinent selections for each class are made, enhancing the representativeness and diversity of the coreset. Furthermore, to ensure that the selected subset informatively represents the entire dataset, we introduce a mathematical tool known as a ‘submodular function,’ as delineated by Krause and Golovin [17]. The function aids in selecting the most informative subset based on the imagewise-classwise average features for each category.

Our empirical evaluations, particularly in scenarios involving the detection of multiple objects, demonstrate the effectiveness of CSOD. For instance, when selecting 200 images from the Pascal VOC dataset [8], our method achieved an impressive improvement of +6.4% point in AP₅₀ compared to random selection. Moreover, we also evaluated it on the BDD100k [33] and MS COCO2017 [18] datasets and confirmed that our method outperforms random selection. These significant achievements emphasize the efficacy and innovativeness of CSOD in addressing the challenges of coreset selection in multi-object image data.

In summary, CSOD represents a pivotal extension of existing coreset selection frameworks to encompass scenarios with multiple objects per image. This approach addresses a gap that traditional methods, which assumed only one object per image, did not cover. While our focus is on multi-objects of the same class, we acknowledge the potential for future expansions of our method to accommodate images featuring various categories of objects. With our unique problem recognition and solution, we aim to shift the paradigm of coreset selection towards more realistic scenarios, specifically image datasets containing multiple objects. This research transcends mere technical advancement, marking a pivotal shift in processing complex real-world datasets and opening new horizons for coreset selection, thereby addressing a significant challenge of the big data era.

2. Background and Prior works

2.1. Coreset selection

Welling [31] introduced the concept of herding for iterative data point selection near class centers. Wei et al. [30] applied the submodular function to the Naïve Bayes and Nearest Neighbor classifier. We also adopt this function, so we provide further explanation in Section 2.3. Braverman et al. [1], Huang et al. [12] modified statistical clustering algorithms like k-median and k-means to identify data points that effectively represent the dataset. Coleman et al. [5] utilized uncertainties measured by entropy or confidence. Huang et al. [13] theoretically explained the upper and lower bounds on the coreset size for k-median clustering in low-dimensional spaces. However, most previous researches focused on image classification, and to the best of our knowledge, our work is the first research to design coreset selection specifically for object detection.

2.2. Dataset Distillation

Coreset Selection and Dataset Distillation are crucial in enhancing model training efficiency, with the former selecting informative data points and the latter synthesizing data to distill the dataset’s information. Despite their different approaches—selection versus synthesis—both methods aim to encapsulate data. Current Dataset Distillation research [3, 7, 20, 28, 35], primarily focused on image classification, presents unexplored potential in object detection. Advancements in Coreset Selection for object detection may have a significant influence on Dataset Distillation strategies for object detection.

2.3. Submodular function

A set function $f : 2^{\mathcal{V}} \rightarrow \mathbb{R}$ is considered submodular if, for any subsets \mathcal{A} and \mathcal{B} of \mathcal{V} where $\mathcal{A} \subseteq \mathcal{B}$ and x is an element not in \mathcal{B} , the following inequality holds:

$$f(\mathcal{A} \cup \{x\}) - f(\mathcal{A}) \geq f(\mathcal{B} \cup \{x\}) - f(\mathcal{B}) \quad (1)$$

Here, $\Delta(x|\mathcal{A}) := f(\mathcal{A} \cup \{x\}) - f(\mathcal{A})$ represents the benefit of adding x to the set \mathcal{A} . In simple terms, this inequality means that adding x to \mathcal{B} provides less additional benefit than adding x to \mathcal{A} . This is because \mathcal{B} already contains some of the information that x can offer to \mathcal{A} . Therefore, we can use submodularity to find a subset that maximizes the benefit of adding each element.

However, in general, selecting a finite subset \mathcal{S} with the maximum benefit is a computationally challenging problem (NP-hard) [17]. To address this, we employ a greedy algorithm that starts with an empty set and adds one element at a time. Specifically, \mathcal{S}_i is updated as $\mathcal{S}_{i-1} \cup \operatorname{argmax}_x \Delta(x|\mathcal{S}_{i-1})$. For more information, please refer to Krause and Golovin [17].

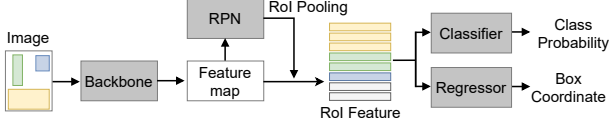


Figure 2. The forward process during the training phase of Faster R-CNN. The RoI features include both foreground and background regions at the forward process.

2.4. Faster R-CNN

Various object detectors exist, including Faster R-CNN [24], SSD [9], YOLO [23], and DETR [2]. We chose Faster R-CNN as our base model. This choice was motivated by its widespread adoption not only in supervised detection but also in various research areas such as few-shot detection [29], continual learning [27], and semi-supervised object detection [15].

Faster R-CNN operates as a two-stage detector. As illustrated in Figure 2, the first stage employs Region Proposal Network (RPN) to generate class-agnostic object candidate regions in the image, followed by pooling these regions to obtain Region of Interest (RoI) feature vectors. In the second stage, the model utilizes these RoI feature vectors for final class prediction and bounding box regression. Our research uses these RoI feature vectors for coresets selection.

2.5. Active Learning for Object Detection

Active learning is concerned with selecting which unlabeled data to annotate and is thus related to coresets selection. In the context of active learning for object detection, Yuan et al. [34] proposed a method based on uncertainty that utilizes confidence scores on unlabeled data. Kothawade et al. [16] aimed to address the low performance issue in rare classes when conducting active learning. The method extracted features of rare classes from labeled data and aimed to maximize the information of rare classes by submodular function and computing the cosine similarity between these labeled features and the features of unlabeled data.

3. Method

3.1. Problem Setup

We have an entire training dataset $\mathcal{T} = \{x_i, y_i\}_{i=1}^D$. Here, $x_i \in \mathcal{X}$ is an input image, and $y_i \in \mathcal{Y}$ is a ground truth. Because these data are for object detection, $y_i = \{c_{i,j}, b_{i,j}\}_{j=1}^{G_i}$ contains variable numbers of annotations depending on the image. In the G_i annotations, $c_{i,j}$ is a class index, and $b_{i,j} = \{b_{i,j}^{left}, b_{i,j}^{top}, b_{i,j}^{right}, b_{i,j}^{bottom}\}$ denotes the coordinates of the j -th bounding box. Coresets selection aims to choose a labeled subset $\mathcal{S} \subset \mathcal{T}$ that best approximates the performance of a model trained on the entire labeled dataset, \mathcal{T} .

In our approach, we prioritize the number of images over

Algorithm 1 CSOD Pseudocode

Require: Training Data $\mathcal{T} = \{(x_i, y_i)\}_{i=1}^D$ with C classes, where $y_i = \{(c_{i,j}, b_{i,j})\}_{j=1}^{G_i}$ and G_i is the number of ground truth objects in the i -th image. Trained backbone f_θ . RoI pooler g . Global Average Pooling function h .

Ensure: Selected subset \mathcal{S} with size N

- 1: Initialize $\mathcal{S}_c = \emptyset, \mathcal{P}_c = \emptyset, \mathcal{Q}_c = \emptyset$ for all $c \in \{1, \dots, C\}$
 - 2: **Stage 1:** Preparing Imagewise-Classwise Features
 - 3: **for** $i = 1$ to D **do**
 - 4: RoI features $\mathcal{R}_i = \{\mathbf{r}_{i,j}\}_{j=1}^{G_i} = h(g(f_\theta(x_i), y_i))$ \triangleright Sec. 3.3
 - 5: **for all** classes c present in y_i **do**
 - 6: $\mathbf{p}_{i,c} = \frac{1}{|\{j|c_{i,j}=c\}|} \sum_{\{j|c_{i,j}=c\}} \mathbf{r}_{i,j}$ \triangleright Sec. 3.4
 - 7: Update $\mathcal{P}_c = \mathcal{P}_c \cup \{\mathbf{p}_{i,c}\}$
 - 8: **end for**
 - 9: **end for**
 - 10: **Stage 2:** Subset Selection
 - 11: **while** $|\mathcal{S}| < N$ **do**
 - 12: **for** $c = 1$ to C **do** \triangleright Sec. 3.5
 - 13: Compute scores $s_{i,c} = \text{score}(\mathbf{p}_{i,c}, \mathcal{Q}_c), \forall i$ \triangleright Eq.4
 - 14: Select the image $i^* = \arg \max_i s_{i,c}$
 - 15: Update $\mathcal{S}_c = \mathcal{S}_c \cup \{(x_{i^*}, y_{i^*})\}$
 - 16: Update $\mathcal{Q}_{c'} = \mathcal{Q}_{c'} \cup \{\mathbf{p}_{i^*,c'}\}, \forall c' \in y_{i^*}$
 - 17: Remove $\mathbf{p}_{i^*,c'}$ from $\mathcal{P}_{c'}, \forall c' \in y_{i^*}$
 - 18: **end for**
 - 19: Update $\mathcal{S} = \bigcup_{c \in \{1, \dots, C\}} \mathcal{S}_c$
 - 20: **end while**
-

the number of annotations. This is because annotations typically consist of relatively few strings, and what primarily affects training time and data storage is the number of images rather than the number of annotations.

3.2. Overview

CSOD picks out the most useful images by looking at one object category at a time. Below are the steps of our CSOD: **Preparing Object Features:** We extract RoI feature vectors from the ground truth of the entire training set (Sec. 3.3). Then, we average the RoI features of the same class within one image (Sec. 3.4).

Choosing the Best Images: We utilize the averaged RoI feature vectors to greedily select images one by one for each class in a rotating manner (Sec. 3.5). In doing so, the submodular optimization technique is introduced to ensure that the selection process considers both representativeness and diversity (Eq. 4). When we pick an image, we do not just use one object in it for training; we use all the objects it contains.

Algorithm 1 provides the pseudocode, while Figure S1 in the supplementary material aids understanding.

3.3. Ground Truth RoI Feature Extraction

With Faster R-CNN, we extract RoI feature vectors from training images by the ground truth (not from the RPN output). If the i -th training image contains G_i ground truth objects, then we have G_i RoI feature vectors, \mathcal{R}_i , as follows:

$$\mathcal{R}_i = \{\mathbf{r}_{i,j}\}_{j=1}^{G_i} = h(g(f_\theta(x_i), y_i)) \quad (2)$$

where x_i is an input image, y_i is a ground truth, f_θ is the backbone trained by the entire data, g is the RoI pooler, h is global average pooling and $r_{i,j}$ is the j -th RoI feature vector of the i -th image.

3.4. Imagewise and Classwise Average

Once we have extracted all the RoI feature vectors for each image, we have a choice to make: For coreset selection, should we average the RoI feature vectors of the same class within a single image to create a single prototype vector representing that class for the image, or should we use these RoI feature vectors directly?

As mentioned in Section 1, we chose the averaging approach. If $\mathcal{R}_i = \{r_{i,j}\}_{j=1}^{G_i}$ represents the RoI feature vectors for the i -th data with G_i ground truth objects, then the average RoI feature vector for class c in the i -th data, denoted as $p_{i,c}$, is calculated as follows:

$$p_{i,c} = \frac{1}{|\{j|c_{i,j} = c\}|} \sum_{\{j|c_{i,j} = c\}} r_{i,j} \quad (3)$$

3.5. Greedy Selection

After obtaining averaged RoI feature vectors, our selection process follows a greedy approach, iteratively choosing one data point from each class at a time. To facilitate this, we compute a similarity-based score for each RoI feature vector. This scoring mechanism based on the submodular function assigns higher scores to RoI feature vectors that are similar to others within the same class and lower scores to those similar to RoI feature vectors that have already been selected. This strategy enables us to take into account previously selected data points when making new selections.

The score function computes the score s for the i -th data point within class c as follows:

$$s_{i,c} = \lambda \cdot \sum_j \text{cos}(p_{i,c}, p_{j,c}) - \sum_j \text{cos}(p_{i,c}, q_{j,c}) \quad (4)$$

The term “cos” represents the cosine similarity, p_i represents the averaged RoI feature vectors that have not been selected yet, and q_i denotes the previously selected RoI feature vectors. The hyperparameter λ is introduced to balance the contributions within the scoring function, in which the former term aims to select the most representative one from among those that have not been selected, while the latter term aims to select something different from what has already been selected before. The experiment related to λ can be found in Section 4.4.2.

CSOD selects data corresponding to the maximum value in Eq. (4) for each class. If a chosen data point includes multiple classes, the features of these classes are considered part of the previously selected q_i . This method systematically cycles through each class, ensuring unique selections, until it reaches the targeted number of choices.

4. Experiments

In this section, we empirically validate the effectiveness of CSOD through experiments. First, we will show that CSOD outperforms various random selections and other coreset selection methods originally designed for image classification. We will then investigate the tendency associated with the number of selected images and the hyperparameter λ of Eq. (4). Additionally, we will compare performance when averaging RoI features of a class within an image versus using individual features as they are. Furthermore, we will extend our analysis to evaluate the performance of different datasets and various network architectures.

4.1. Implementation details

We conducted experiments on Pascal VOC 2007+2012 [8], using the trainval set for selection and training, and the VOC07 test set for evaluation. The metric is Average Precision at IoU 0.5 (AP_{50}). For ablation and analysis, we chose 200 images from 20 classes, training for 1000 iterations. We averaged performance over 20 runs due to the limited number of images. We used Faster R-CNN-C4 [24] with ResNet50 [11]. For the selection phase, we used the model weight trained on VOC07+12, provided by detectron2 [32]. After selection, a new model was trained on the chosen subset, with a backbone pre-trained on ImageNet [6]. For further details, see Section S1 in the supplementary material.

4.2. Comparison with Other Selections

Comparison Targets. Table 1 shows the comparison list. Random refers to the method where one image per class is randomly selected in turn. There can be multiple classes in a single image, and when selecting in turn by class, the images were chosen without duplication to make the target number of images. Additional experiments regarding Random Selection are conducted in Section 4.3.

Coreset selection methods for image classification, such as Herding [31], k-Center Greedy [25], and Submodular function [14], were also compared. The CSOD’s network weight was employed, and the backbone feature was globally average pooled to utilize that feature vector for selection. Similar to random selection, images were evenly chosen from each class.

Result. As seen in Table 1, our method consistently shows the highest results. Random selection shows higher performance than some existing methods, which implies that these methods are designed only for the image classification task and yield lower results in object detection. The submodular function showed some effectiveness when the number of data was low. However, as mentioned in Section 1 and Figure 1, it is a modeling that fundamentally cannot consider multiple objects of various sizes and locations. Therefore, it not only showed lower results than random when selecting over 500 images but also significantly lower results than

Selection Method	20	100	200	500	1000
Random (Uniform)	9.8 \pm 2.2	27.9 \pm 1.6	37.9 \pm 1.1	50.7 \pm 1.0	58.4 \pm 0.6
Herding [31]	4.1 \pm 0.7	17.7 \pm 1.2	26.0 \pm 0.8	37.8 \pm 0.7	46.4 \pm 0.7
k-Center Greedy [25]	10.0 \pm 1.3	21.8 \pm 2.1	32.3 \pm 0.9	47.4 \pm 1.0	55.9 \pm 0.3
Submodular Function [14]	12.9 \pm 0.9	30.5 \pm 1.3	38.6 \pm 0.9	48.8 \pm 0.7	55.8 \pm 0.3
CSOD (Ours)	14.5 \pm 1.6	34.4 \pm 1.0	44.3 \pm 0.7	54.1 \pm 0.7	60.6 \pm 0.4

Table 1. Comparison with random and coreset selection for image classification, reporting AP₅₀ on the VOC07 test data. We ran all experiments 20 times, with \pm indicating standard deviation. Note that the standard deviation is so small that the performance gap is clear. Herding, Submodular, and CSOD select subsets deterministically, with only network weight initialization affected by random seeds.

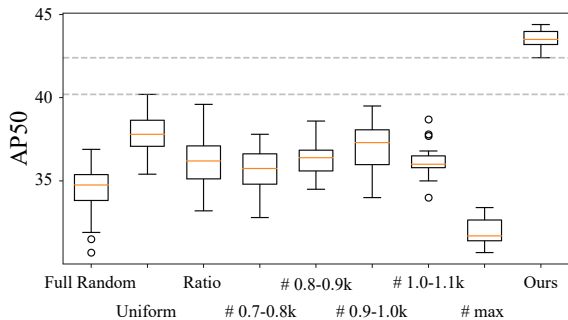


Figure 3. Comparison with various selection methods. ‘#’ denotes the number of objects in the selected data.

CSOD. Based on these results, future experiments for comparison will be conducted with Random selection.

4.3. Comparison with Random Selections

Figure 3 shows that our approach consistently outperforms other selection methods when selecting 200 images. Notably, in this comparison, “# max” and “Ours” are the only methods without randomness, while the rest incorporate some degree of randomness. Therefore, we did not specifically address the performance variance of each selection method. Our method was implemented with a fixed set and without randomness, leading to reduced performance variance only comes from the training process. This experiment’s significance lies in the clearly higher performance of ours compared with those of other methods.

We categorized random selection into several methods. “Full random” selects 200 images randomly, but repeats the process if any classes have no objects in those 200 images. “Uniform” and “Ratio” involve sampling images one by one for each class until 200 images are selected (sampling without replacement). In these cases, images selected from one class are excluded from selection in other classes, as an image can contain objects in multiple classes. “Uniform” distributes images evenly with 10 per class, while “Ratio” selects images based on the proportion of images per class.

The CSOD result consists of 1,032 annotations. Therefore, we also experimented with random selection while

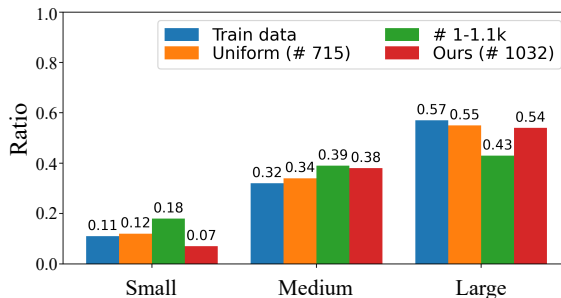


Figure 4. Ratio of box sizes. We followed the size criteria provided by VOC. ‘#’ denotes the number of objects in the selected data.

controlling for the number of annotations. “# 700-1100” limits annotations to this range using the Uniform method. “# max” also follows Uniform but selects images based on the annotation count in descending order rather than selecting them randomly.

4.3.1 The performance and object size ratio.

Figure 4 shows the relationship between box size, object count, and performance. We conducted two comparisons. First, we compared Uniform and CSOD. We observed that the ratio of Uniform was closer to that of the entire dataset in terms of KL divergence, while Ours had more annotations. Second, we compared CSOD and “# 1-1.1k”. Both methods had similar object counts, but CSOD’s box size ratio was closer to that of the training data. While we cannot definitively assert causality, it appears that a well-represented subset with an equal number of images has a correlation with both box size and object count.

4.4. Analysis of the number of images and the hyperparameter λ

4.4.1 The number of selected images

Figure 5 shows performance with the number of selected images. Since selecting 20 images indicates only one image per class is selected, λ is meaningless. For other cases (100, 200, 500, and 1000), we set λ as (0.0125, 0.04375, 0.0625,

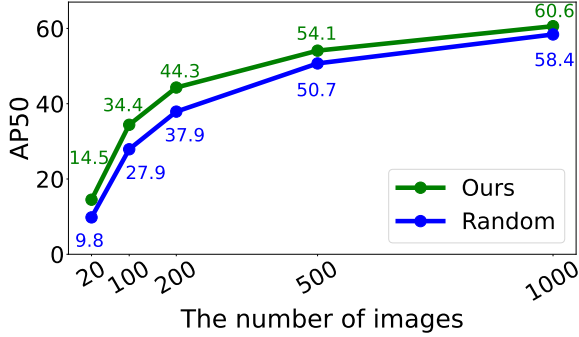


Figure 5. Performance according to the selected image counts.

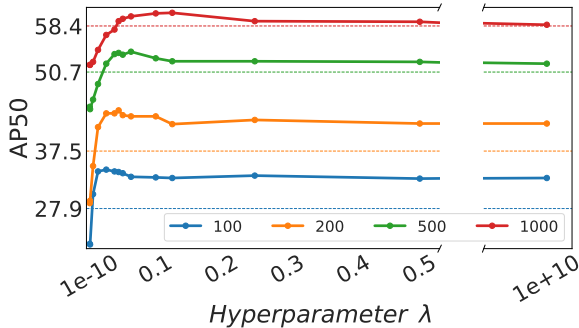


Figure 6. AP_{50} and λ . Dashed lines represent random selection performance.

and 0.025), respectively. Compared to the random selection, we observe that as the number of selected images increases, the performance gap naturally decreases, but it consistently remains at a high level.

4.4.2 Balance hyperparameter λ

Figure 6 illustrates the relationship between performance and λ in Eq. (4). A high λ value ($1e+10$) means selecting images based solely on cosine similarity, prioritizing representative images. In contrast, a small λ value ($1e-10$) means selecting an image per class with the highest cosine similarity first and then selecting images that are as dissimilar as possible from those already selected. In other words, it emphasizes diversity from a cosine similarity viewpoint.

The observations can be made: Firstly, our approach outperforms random selection when λ is above a certain threshold. Secondly, it is better to consider both representativeness and diversity by appropriately tuning λ rather than simply selecting images purely based on the order of cosine similarity ($1e+10$). Lastly, the optimal λ value varies depending on the number of images to be selected, as the greedy selection process (Section 3.5) progressively increases the number of selected images. Please refer to Table S1 in the supplementary material for the AP_{50} values corresponding to the λ values.

		The number of changes in the image list				
		0	18	32	45	113
Objectwise	λ	$1e+10$	0.125	0.075	0.051	0.015
	AP_{50}	40.4	40.3	40.7	41.4	39.0
Imagewise (Ours)	λ	$1e+10$	0.100	0.050	0.038	0.013
	AP_{50}	42.1	43.3	43.5	43.8	41.5

Table 2. Comparison with two methods, “Imagewise” (averaging RoI vectors) and “Objectwise” (not averaging), for selecting 200 images. The number of changes in the image list is based on $\lambda = 1e + 10$ as the reference point (The smaller λ , the severer the change). λ is rounded to the fourth decimal place.

	20	40	60	80	100	200
Objectwise	13.0	20.6	25.8	29.1	31.5	40.4
Imagewise (Ours)	14.2	23.1	27.3	30.1	32.9	42.1

Table 3. λ is $1e+10$ in all cases, meaning that we selected based solely on cosine similarity ranking.

4.5. Effectiveness of Averaging RoI feature vectors

4.5.1 Performance comparison

Table 2 compares performance between averaging the RoI feature vectors of the same class (Imagewise) or not (Objectwise). These two cases have different balance strengths for λ , as Imagewise averages within the same class, resulting in significantly fewer RoI feature vectors. Therefore, we compared the extent to which the image list changes, using $1e+10$ as the reference point. Remarkably, we observed consistent high performance regardless of λ values. However, even Objectwise outperformed random selection, achieving a result higher than 37.5 of random selection.

4.5.2 Representativeness: Objectwise vs. Imagewise feature vector

Table 3 compares Objectwise and Imagewise based on the number of selected images when $\lambda=1e+10$. This experiment highlights that even if the cosine similarity of a single object within an image is exceptionally high, that image may not effectively represent the overall distribution of the data. For example, the case where only one image per class is selected (20 in the table) indicates how well a single image represents the corresponding class. The table shows the superiority of our imagewise selection over objectwise selection.

4.5.3 Visualization of objectwise selection

Figure 7 illustrates a limitation of the objectwise approach, where the selected image may not effectively represent the



Figure 7. Examples of the Objectwise selection. Top: ‘car’ class. Bottom: ‘person’ class. The red dotted boxes indicate objects with low rankings in Eq. (4).

entire dataset. Even if an image is selected because it contains an object with high cosine similarity, it does not guarantee that other objects within the same image will have similarly high cosine similarities. In other words, the cosine similarity of one object in an image with all the other objects in the entire dataset may not accurately represent the cosine similarities of all objects in that image.

4.5.4 Why imagewise (averaging) selection over objectwise selection?

Let us compare object counts and size ratios in Section 4.3.1. In our Imagewise approach, there are 1,032 objects in our 200 selected images, which is higher than 806 in the Objectwise approach. Additionally, when considering the size ratios (small, medium, large), the Imagewise approach results in (7.3%, 38.2%, 54.5%), which is closer to the large object ratio in the entire train data, (10.5%, 32.0%, 57.5%), compared to the Objectwise, (10.2%, 37.2%, 52.6%). When we calculated the KL divergence between the distributions of the selected images and the entire training data, we found that Objectwise had a KL divergence of 0.006, lower than Imagewise’s 0.013.

Object count	1	2-4	5 or more
Large	0.866	0.931	0.939
Medium	0.862	0.915	0.931
Small	0.798	0.818	0.831

Table 4. Cosine similarity between the entire average features and the average feature of each image by size in the ‘person’ class.

This suggests that the number of annotations played a more significant role in the performance than the size ratio in the case of Imagewise and Objectwise. Despite the higher KL divergence for Ours, there were substantial differences in the number of annotations for each size. Ours had counts of (75, 395, 562) for each size, whereas Objectwise had counts of (82, 300, 424).

We formulated a hypothesis that “As the number of objects within an image increases and their sizes are larger, the cosine similarity between the class’s entire average RoI vector (class prototype) and the image’s average RoI vector (image prototype) for that class will be higher.”

To validate this hypothesis, we conducted the experiment presented in Table 4. Initially, we averaged all RoI vectors for the ‘person’ class (class prototype). Then, we made an averaged RoI vector by size within each image (imagewise-size-wise prototype). We subsequently computed the cosine similarity between the class prototype and the imagewise-size-wise prototypes. The results confirmed that the Imagewise approach leads to a higher selection of larger objects, resembling the entire dataset.

4.6. Evaluation on the BDD100k dataset

BDD100k [33] is a significant dataset for autonomous driving, consisting of 100k images, 1.8M annotations, and 10 different classes. Following the official practice, we split the dataset into 70k for training with 1.3M annotations. Table 5 shows the results on the validation data, illustrating that our method consistently achieves higher AP₅₀, AP₇₅, and AP compared to random selection. Notably, similar performance improvements were observed in our experiments with the VOC dataset. However, BDD100k, explicitly designed for real-world autonomous driving applications, offers a more challenging and realistic benchmark. The fact that our method excels even in the challenging environment of BDD100k further demonstrates its effectiveness and practicality. For implementation details, kindly refer to Section S2 in the supplementary material.

4.7. Evaluation on the COCO dataset

The COCO2017 dataset [18] encompasses 80 classes, partitioned into 118K images for the training set and 5K for the validation set. Experiments were conducted with subsets of 400 and 800 images selected from the training data. Table 6

	num img	AP ₅₀	AP ₇₅	AP
200	Random	25.8	9.7	12.0
	Ours	29.0	10.8	13.5
	Δ	+3.2	+1.1	+1.5
500	Random	32.2	13.4	15.8
	Ours	35.1	14.9	17.5
	Δ	+2.9	+1.5	+1.7
1000	Random	37.1	16.2	18.6
	Ours	39.4	17.8	20.1
	Δ	+2.3	+1.6	+1.5
2000	Random	42.1	19.7	22.0
	Ours	43.7	21.0	23.2
	Δ	+1.6	+1.3	+1.2

Table 5. BDD100k result

	num img	AP ₅₀	AP ₇₅	AP
400	Random	15.1	4.9	6.6
	Ours	16.7	5.8	7.5
	Δ	+1.6	+0.9	+0.9
800	Random	19.4	7.5	9.1
	Ours	20.1	8.2	9.6
	Δ	+0.7	+0.7	+0.5

Table 6. COCO2017 result

shows the outcomes for the validation set. Despite the substantially larger size of the dataset compared to VOC, it was observed that our method was effective. For reproducibility please refer to Section S3 in the supplementary material.

The BDD dataset has more annotations despite having fewer images compared to COCO. Interestingly, the performance improvement margin on COCO was smaller than on BDD. This observation raises several points for consideration. The BDD dataset, focused on autonomous driving, predominantly encompasses outdoor scenes with less diversity, such as perspective, compared to COCO. Conversely, COCO spans a wider spectrum, including both indoor and outdoor scenes and a larger variety of classes. This diversity potentially renders the accurate representation of the entire data distribution with a subset of images more challenging. This observation not only clarifies our current results but also highlights this as a key area for future study.

4.8. Cross-architecture evaluation

Table 7 presents an experiment in which we assessed whether the 500 images selected using Faster R-CNN remained effective for different networks, namely RetinaNet [19] and FCOS [26]. We were able to confirm the effectiveness of images selected with Faster R-CNN for other networks as well. Unlike Faster R-CNN, these two networks often encountered training issues due to loss explo-

	RetinaNet	FCOS
random	54.5	47.9
ours	58.3	53.1
Δ	+3.8	+5.2

Table 7. Cross architecture experiment. We trained the models on 500 VOC images and reported AP₅₀.

sion when following their respective default hyperparameters. Therefore, we adjusted the hyperparameters, such as the learning rate and gradient clipping, but it is important to note that the hyperparameters for random selection and our method remained consistent. Please refer to Section S4 in the supplementary material for reproducibility.

5. Discussion

Conclusion. We have proposed a Coreset selection method for Object Detection tasks, addressing the unique challenges presented by multi-object and multi-label scenarios. This stands in contrast to traditional image classification approaches. Our approach considers both representativeness and diversity while taking into account the difficulties we have outlined in Section 1 and illustrated in Figure 1. Through experiments, we have demonstrated the effectiveness of our method, and its applicability to various architectures. We hope this research will further develop and find applications in diverse areas, such as dataset distillation.

Limitation. While our research leveraged RoI features from ground truth boxes and achieved promising results, it is important to note certain limitations. Firstly, we did not explicitly incorporate background features, which could provide additional context and potentially enhance coreset selection in object detection. Future research could explore the explicit utilization of background features. Our approach, which selects greedily on a class-by-class basis, can take into account the RoI features of the current class even when they were selected during the turn of other classes. However, our method does not simultaneously incorporate the features of other classes within the same image. Further research could explore ways to capture interactions between different classes more effectively within a single image.

Future work. Since CSOD considers localization, there may be aspects that can be applied to other tasks related to localization, such as 3D object detection. Furthermore, while dataset distillation has predominantly been studied in the context of image classification, it could also become a subject of research in the field of object detection datasets.

Acknowledgements. This work was supported by NRF grant (2021R1A2C3006659) and IITP grants (2022-0-00953, 2021-0-01343), all funded by MSIT of the Korean Government.

References

- [1] Vladimir Braverman, Shaofeng H-C Jiang, Robert Krauthgamer, and Xuan Wu. Coresets for ordered weighted clustering. In *International Conference on Machine Learning*, pages 744–753. PMLR, 2019. 1, 2
- [2] Nicolas Carion, Francisco Massa, Gabriel Synnaeve, Nicolas Usunier, Alexander Kirillov, and Sergey Zagoruyko. End-to-end object detection with transformers. In *European conference on computer vision*, pages 213–229. Springer, 2020. 3
- [3] George Cazenavette, Tongzhou Wang, Antonio Torralba, Alexei A Efros, and Jun-Yan Zhu. Dataset distillation by matching training trajectories. In *Proceedings of the IEEE/CVF Conference on Computer Vision and Pattern Recognition*, pages 4750–4759, 2022. 2
- [4] Bowen Cheng, Ishan Misra, Alexander G. Schwing, Alexander Kirillov, and Rohit Girdhar. Masked-attention mask transformer for universal image segmentation. 2022. 1
- [5] Cody Coleman, Christopher Yeh, Stephen Mussmann, Baharan Mirzasoleiman, Peter Bailis, Percy Liang, Jure Leskovec, and Matei Zaharia. Selection via proxy: Efficient data selection for deep learning. *arXiv preprint arXiv:1906.11829*, 2019. 1, 2
- [6] J. Deng, W. Dong, R. Socher, L.-J. Li, K. Li, and L. Fei-Fei. ImageNet: A Large-Scale Hierarchical Image Database. In *CVPR*, 2009. 4
- [7] Tian Dong, Bo Zhao, and Lingjuan Lyu. Privacy for free: How does dataset condensation help privacy? In *International Conference on Machine Learning*, pages 5378–5396. PMLR, 2022. 2
- [8] Mark Everingham, Luc Van Gool, Christopher KI Williams, John Winn, and Andrew Zisserman. The pascal visual object classes challenge 2007 (voc2007) results. 2007. 2, 4
- [9] Cheng-Yang Fu, Wei Liu, Ananth Ranga, Amrith Tyagi, and Alexander C Berg. Dssd: Deconvolutional single shot detector. *arXiv preprint arXiv:1701.06659*, 2017. 3
- [10] Chengcheng Guo, Bo Zhao, and Yanbing Bai. Deepcore: A comprehensive library for coreset selection in deep learning. In *International Conference on Database and Expert Systems Applications*, pages 181–195. Springer, 2022. 1, 3
- [11] Kaiming He, Xiangyu Zhang, Shaoqing Ren, and Jian Sun. Deep residual learning for image recognition. In *CVPR*, pages 770–778, 2016. 4
- [12] Lingxiao Huang, Shaofeng Jiang, and Nisheeth Vishnoi. Coresets for clustering with fairness constraints. *Advances in Neural Information Processing Systems*, 32, 2019. 2
- [13] Lingxiao Huang, Ruiyuan Huang, Zengfeng Huang, and Xuan Wu. On coresets for clustering in small dimensional euclidean spaces. *arXiv preprint arXiv:2302.13737*, 2023. 2
- [14] Rishabh Iyer, Ninad Khargoankar, Jeff Bilmes, and Himanshu Asanani. Submodular combinatorial information measures with applications in machine learning. In *Algorithmic Learning Theory*, pages 722–754. PMLR, 2021. 4, 5
- [15] Jisoo Jeong, Seungeui Lee, Jeessoo Kim, and Nojun Kwak. Consistency-based semi-supervised learning for object detection. *Advances in neural information processing systems*, 32, 2019. 3
- [16] Suraj Kothawade, Saikat Ghosh, Sumit Shekhar, Yu Xiang, and Rishabh Iyer. Talisman: targeted active learning for object detection with rare classes and slices using submodular mutual information. In *European Conference on Computer Vision*, pages 1–16. Springer, 2022. 3, 4
- [17] Andreas Krause and Daniel Golovin. Submodular function maximization. *Tractability*, 3(71-104):3, 2014. 2
- [18] Tsung-Yi Lin, Michael Maire, Serge Belongie, James Hays, Pietro Perona, Deva Ramanan, Piotr Dollár, and C Lawrence Zitnick. Microsoft coco: Common objects in context. In *European conference on computer vision*, pages 740–755. Springer, 2014. 2, 7
- [19] Tsung-Yi Lin, Priya Goyal, Ross Girshick, Kaiming He, and Piotr Dollár. Focal loss for dense object detection. In *Proceedings of the IEEE international conference on computer vision*, pages 2980–2988, 2017. 8
- [20] Timothy Nguyen, Roman Novak, Lechao Xiao, and Jaehoon Lee. Dataset distillation with infinitely wide convolutional networks. *Advances in Neural Information Processing Systems*, 34:5186–5198, 2021. 2
- [21] Kemal Oksuz, Baris Can Cam, Sinan Kalkan, and Emre Akbas. Imbalance problems in object detection: A review. *IEEE transactions on pattern analysis and machine intelligence*, 43(10):3388–3415, 2020. 3
- [22] Alec Radford, Jong Wook Kim, Chris Hallacy, Aditya Ramesh, Gabriel Goh, Sandhini Agarwal, Girish Sastry, Amanda Askell, Pamela Mishkin, Jack Clark, et al. Learning transferable visual models from natural language supervision. In *International conference on machine learning*, pages 8748–8763. PMLR, 2021. 1
- [23] Joseph Redmon and Ali Farhadi. Yolov3: An incremental improvement. *arXiv preprint arXiv:1804.02767*, 2018. 3
- [24] Shaoqing Ren, Kaiming He, Ross Girshick, and Jian Sun. Faster r-cnn: Towards real-time object detection with region proposal networks. In *NIPS*, pages 91–99, 2015. 3, 4
- [25] Ozan Sener and Silvio Savarese. Active learning for convolutional neural networks: A core-set approach. *arXiv preprint arXiv:1708.00489*, 2017. 4, 5
- [26] Zhi Tian, Chunhua Shen, Hao Chen, and Tong He. Fcos: Fully convolutional one-stage object detection. In *Proceedings of the IEEE/CVF international conference on computer vision*, pages 9627–9636, 2019. 8
- [27] Jianren Wang, Xin Wang, Yue Shang-Guan, and Abhinav Gupta. Wanderlust: Online continual object detection in the real world. In *Proceedings of the IEEE/CVF international conference on computer vision*, pages 10829–10838, 2021. 3
- [28] Tongzhou Wang, Jun-Yan Zhu, Antonio Torralba, and Alexei A Efros. Dataset distillation. *arXiv preprint arXiv:1811.10959*, 2018. 2
- [29] Xin Wang, Thomas E Huang, Trevor Darrell, Joseph E Gonzalez, and Fisher Yu. Frustratingly simple few-shot object detection. *arXiv preprint arXiv:2003.06957*, 2020. 3
- [30] Kai Wei, Rishabh Iyer, and Jeff Bilmes. Submodularity in data subset selection and active learning. In *International conference on machine learning*, pages 1954–1963. PMLR, 2015. 2

- [31] Max Welling. Herding dynamical weights to learn. In *Proceedings of the 26th Annual International Conference on Machine Learning*, pages 1121–1128, 2009. [2](#), [4](#), [5](#)
- [32] Yuxin Wu, Alexander Kirillov, Francisco Massa, Wan-Yen Lo, and Ross Girshick. Detectron2. <https://github.com/facebookresearch/detectron2>, 2019. [4](#)
- [33] Fisher Yu, Haofeng Chen, Xin Wang, Wenqi Xian, Yingying Chen, Fangchen Liu, Vashisht Madhavan, and Trevor Darrell. Bdd100k: A diverse driving dataset for heterogeneous multitask learning. In *Proceedings of the IEEE/CVF conference on computer vision and pattern recognition*, pages 2636–2645, 2020. [2](#), [7](#)
- [34] Tianning Yuan, Fang Wan, Mengying Fu, Jianzhuang Liu, Songcen Xu, Xiangyang Ji, and Qixiang Ye. Multiple instance active learning for object detection. In *Proceedings of the IEEE/CVF Conference on Computer Vision and Pattern Recognition*, pages 5330–5339, 2021. [3](#)
- [35] Yongchao Zhou, Ehsan Nezhadarya, and Jimmy Ba. Dataset distillation using neural feature regression. *Advances in Neural Information Processing Systems*, 35:9813–9827, 2022. [2](#)
- [36] Zhuofan Zong, Guanglu Song, and Yu Liu. Detsr with collaborative hybrid assignments training, 2022. [1](#)

Coreset Selection for Object Detection

Supplementary Material

S1. Additional implementation details

Section 4.1 describes implementation details, and here we introduce additional implementation details. During training with the selected data, we used the SGD optimizer with a learning rate of 0.02, weight decay of 0.0001, and momentum of 0.9. The number of iterations was as follows: When the number of images was 200 or fewer, we trained the initialized network for 1000 iterations. For 500 images, we trained it for 2000 iterations. With 1000 images, we trained it for 4000 iterations. When there were 200 images or fewer, we performed training on the initialized network for 1000 iterations to ensure loss convergence. The learning rate was reduced to 0.1 times the initial value at 80% of the training iterations. The warm-up was conducted for 100 iterations, and there was no gradient clipping.

Regarding image sizes, we resized the shorter side to 800 pixels and maintained the original aspect ratio, ensuring the longer side remained below 1333 pixels. During training, resizing was done within the range of (480-800) with a step size of 32.

S2. BDD100k experiment detail

Like Pascal VOC, we experimented with Faster R-CNN-C4 with ResNet50. For the VOC experiment, we used the Faster R-CNN weight provided by detectron2. However, for the BDD experiment, there was no weight provided by detectron2. Therefore, we used ImageNet pretrained backbone to train the Faster R-CNN on the train data. We trained with a max iteration of 90k and a learning rate decay at 60k and 80k. The rest, like SGD, learning rate, and data augmentation strategy, was the same with VOC.

We initially sampled 5,000 images for each class and then ran our method. For more on this setting, please refer to Section S5. For the balance hyperparameter λ of Eq. (4), we set them to (0.075, 0.0675, 0.1, 0.1875) for the images (200, 500, 1000, 2000), respectively. After selection, we trained the selected subset during 4k iteration for 200 images, 4k iteration for 500 images, 8k iteration for 1000 images, and 8k iteration for 2000 images. And, the learning rate was decayed at 80% of the max iteration.

S3. COCO2017 experiment detail

Like Pascal VOC, we experimented with Faster R-CNN-C4 with ResNet50. Similar to VOC, we used the Faster R-CNN weight provided by detectron2 for selection.

We initially sampled 30,000 images for each class and then ran our method. For more on this setting, please re-

fer to Section S5. For the balance hyperparameter λ of Eq. (4), we set them to (400, 800) for the images (0.05, 0.1), respectively. After selection, we trained the selected subset during 4k iteration for 400 images and 8k iteration for 800 images. And, the learning rate was decayed at 80% of the max iteration.

S4. Cross architecture detail

In the case of RetinaNet and FCOS, as mentioned in Section 4.8, following the configurations of each detector or the configurations we experimented with in Faster R-CNN resulted in significant training instability due to loss explosion. Therefore, when training with 500 images, we followed these hyperparameters: We increased the number of training iterations from 2000 to 6000, matching the learning rate decay point at 5,200 iterations accordingly. The learning rate for RetinaNet was set to 0.01, following Detectron2, while for FCOS, it was reduced from 0.01 to 0.005. We extended the warm-up iteration from 100 to 1000 iterations. Gradient clipping was introduced with a threshold of 1.0, which was previously absent. We reduced the image size in training and testing, scaling down the shorter side from 800 to 600 pixels and the longer side from 1333 to 1000 pixels. We also reduced the data resize augmentation range from 480-800 to 360-600. For other network hyperparameters, we followed Detectron2's settings for RetinaNet and used the official code's configurations for FCOS.

S5. Sampling first, then selection for reducing cosine similarity calculation

Table S2 presents the experiment that we first reduced the number of data per class by random selection and then applied our method. Note that the numbers per class are not precisely equal, as some images might contain multiple classes, but rather approximations. We conducted this experiment for two reasons: handling classes with a large number of images, which can make cosine similarity calculations time-consuming, and addressing class imbalance.

Our results show a clear trend. Even with just 50 images per class, our algorithm outperformed random selection by a significant margin. Moreover, increasing the sample size to 1,000 images per class yielded similar performance. This implies that, even when dealing with classes with an unusually high number of images, as long as computational resources allow, sampling without replacement is expected to provide markedly better results than random selection. For reference, the minimum, maximum, and average number of images per class are 423, 6,469, and 1,281, respectively.

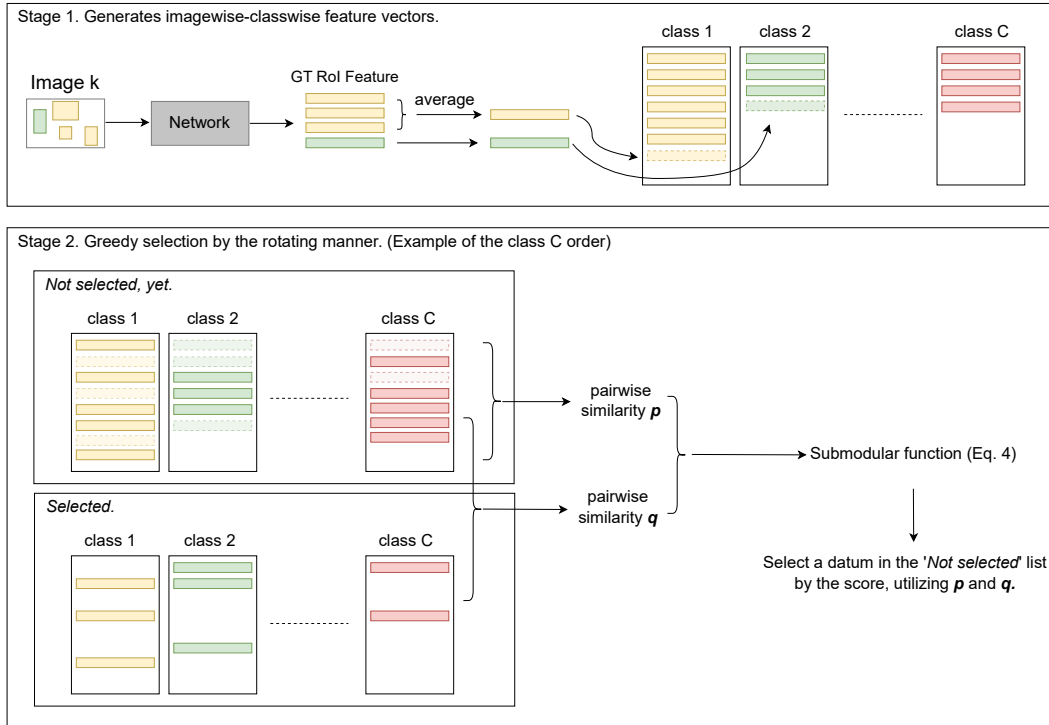


Figure S1. Stage 1 is to create imagewise-classwise feature vectors by applying RoI pooling to the ground truth boxes and subsequently averaging them by class. In Stage 2, illustrated by class C as an example, data selection for each class is performed. It calculates scores that consider the balance between previously selected and the not-selected data (Eq. 4). After selection by Eq. 4, the datum selected in the current selection step is popped from the 'Not selected, yet' list and inserted into the 'Selected' list. After selecting a datum for class C, the process returns to class 1 and repeats the same steps until the desired number of images is reached.

count	1e-10	0.0005	0.005	0.0125	0.025	0.0375	0.04375	0.05	0.0625	0.1	0.125	0.25	0.5	1e+10
100	22.0	21.9	30.3	34.1	34.4	34.1	34.0	33.8	33.2	33.1	33.0	33.4	32.9	33.0
200	28.8	29.2	35.0	41.5	43.8	43.8	44.3	43.5	43.3	43.3	42.0	42.7	42.1	42.1
500	44.9	44.5	46.1	48.7	52.1	53.7	53.9	53.6	54.1	53.0	52.5	52.5	52.4	52.1
1000	51.9	51.9	52.4	54.4	56.9	57.8	59.2	59.6	60.0	60.5	60.6	59.2	59.1	58.6

Table S1. AP_{50} on Pascal VOC. The optimal λ increases as the number of images grows.

Random	The number of sampled image per class								Ours
	50	100	200	300	400	500	1000		
AP_{50}	37.5	42.0	42.8	43.6	43.9	43.9	43.5	44.0	44.3

Table S2. Coreset Selection after Sampling. In all cases, we ultimately selected 200 images.

S6. Analysis of the ratio of classwise annotation counts

We explored how selection methods affect the class balance of annotations. Figure S2 shows the results. Note that in this analysis, we considered the proportions without considering the number of annotations or object sizes.

When we calculated the KL divergence with the train data, Full Random appeared to be the closest. We also evaluated how balanced the class ratios were based on the entropy. Our method showed the best balance in terms of the entropy.

Intuitively, we might expect the performance to be better when the subset's class ratios are closest to those in the train data. However, this was not necessarily the case, suggesting two possibilities. First, the number of annotations in the subsets is significantly smaller than in the train data. Therefore, having a relatively balanced dataset, even if it differs from the train data's class ratios, could be more beneficial for learning. Second, as shown in Section 4.3.1, the size of objects or the number of annotations might significantly impact performance.

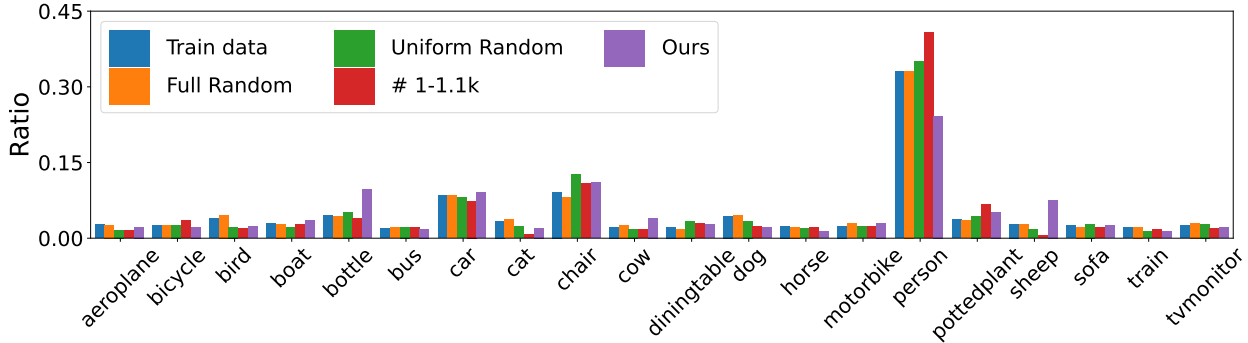


Figure S2. Annotation ratios for each class. When considering the KL divergence as the criterion with train data, Full Random was the closest. However, when calculating the balance level by computing the entropy, Ours showed the most balance.

S7. Coreset selection with gradients instead of RoI features

In our pursuit of selecting an informative subset for training, we conducted an experimental comparison where we explored the use of gradient vectors derived from RoI feature vectors instead of directly employing the RoI feature vectors. This approach was motivated by [10], where they demonstrated the effectiveness of gradients in image classification tasks.

The gradient vectors were obtained by backpropagating from the classification loss. Furthermore, we performed our method with the gradient of RoI feature vectors instead of RoI feature vectors. We focused solely on the gradients of classification loss because they have significantly higher dimensions than RoI feature vectors, mainly due to the multiplication of the number of classes.

In our experiments, when selecting 200 images with λ set to 0.05, we compared the AP_{50} values. Results revealed that utilizing our method with RoI feature vectors achieved an AP_{50} of 43.5, whereas when using gradients, the AP_{50} was 42.3.

S8. Class-specific hyperparameter λ set differently for each class

We experimented with setting λ of Eq. (4) differently for each class. Because the number of objects varies among classes, it leads to varying scales in the former term of the right-hand side of Eq. (4).

So, if we denote the number of objects in class c as N_c , we conducted hyperparameter tuning for λ_c , such as $\lambda_c \propto 1/N_c$, $\lambda_c \propto 1/\log_2(N_c)$, or $\lambda_c \propto 1/a^{N_c}$, where a is a hyperparameter. However, we observed no significant difference in AP_{50} . Furthermore, class-specific AP_{50} values did not reveal any consistent trends concerning the number of objects.

There are several possible explanations to consider. First,

our method selects classes independently, without considering other classes. However, as mentioned in Section 1, a single image can contain multiple classes. Therefore, the assumption of complete independence among classes may not hold, and λ_c may have indirectly influenced other classes. Second, the VOC dataset exhibits a relatively less severe class imbalance compared to other datasets [21]. Based on our observations that there is not a significant performance difference within a specific range of λ values, it is possible that the imbalance is not severe.

Data imbalance is a challenging yet crucial issue addressed in many domains. Coreset selection from imbalanced data is also an area that deserves deeper exploration in the future.

S9. What would happen if we discarded all the selected images and chose again?

We observed an AP_{50} of 43.5 when we set λ to 0.05 and selected 200 images, with 10 images per class in the VOC dataset. Subsequently, we conducted an additional experiment in which we excluded the originally chosen 200 images and then selected another 200 images. In this case, the AP_{50} value was 42.2.

Two crucial observations emerged from these results: Firstly, the initial selection of 200 images effectively represented the entire dataset. Secondly, even when we reselected 200 images from the remaining dataset after discarding the initial selection, the performance remained significantly superior to random selection, which yielded an AP_{50} of 37.5.

S10. Measurement of CSOD’s selection Time

Table S3 presents the results of measuring the time it takes for CSOD to select data. The time taken to select VOC in Section 4.2 was measured, and the time for selecting BDD in Section 4.6 was measured. As the results indicate, there is a tendency for the time to increase linearly with the number of selected images. And, comparing BDD and VOC, the

Dataset	The number of selected images			
	200	500	1000	2000
VOC	15	42	80	158
BDD	310	712	1393	2824

Table S3. Selection time measurement result. When measuring, it was measured using CPU, not GPU. The unit is second.

more data there is, the longer it takes to make a selection. This linear increase in time is not a drawback but rather an expected and manageable aspect of the process, ensuring a thorough and proportional selection as the volume of data scales up.

S11. Comparative and adaptation study utilizing active learning for object detection

Talisman [16] applied submodular functions in the context of active learning. Talisman focuses on maximizing the performance of rare classes in active learning for object detection. Therefore, when provided with both labeled and unlabeled data, their goal is to select unlabeled data that maximizes the information about rare objects within the labeled data. While our objectives and methods are entirely different from the paper, we share a commonality in the use of submodular functions.

The main differences in the procedures of Talisman and CSOD are as follows: First, Talisman starts by randomly selecting N objects from each category, while CSOD does not follow this initial step. Second, Talisman searches for images containing at least one object that maximizes the information given the initial set of N objects. This process uses a method known as a submodular function. It's important to understand that Talisman selects these images based on the presence of a single object that greatly enriches the information content, regardless of how similar or dissimilar the other objects in the image are.

Kindly note that this succinct overview provides only a glimpse of the procedural differences, and it's crucial to recognize that the two works are guided by distinct objectives, leading to fundamentally different frameworks. Nevertheless, we adapted Talisman to our problem formulation and conducted an experiment to select 200 images from Pascal VOC.

We made several modifications to tailor the Talisman method to our needs:

- While Talisman primarily focused on rare classes, we extended its application to all classes in our problem.
- Instead of generating RoI features from unlabeled data using RPN outputs, we changed it for creating RoI features from Ground Truth (GT) boxes, given our supervised set-

ting.

- The Talisman algorithm initially started with a few labeled rare objects. Our adaptation altered the method to start with three random images per class from the entire dataset. For a fair comparison, CSOD also started with the first three images identical to Talisman.

As a result, AP_{50} of our adaptation of Talisman was 39.3. This result was higher than the random selection of 37.5 but lower than 43.1 of ours, which started with the first three images identical to Talisman.